World Cancer Research Journal
WCRJ 2025; 12 : e2913
DOI: doi.org/10.32113/WCRJ_20257_2913

EXPLORING THE ANTI-TUMOR MECHANISMS OF *ANTHRISCUS SYLVESTRIS* USING A NETWORK PHARMACOLOGY AND MOLECULAR DOCKING APPROACH

J. Z. SHU[1], Y. JIANG[2], H. Z. CHEN[2], F. Y. LIU[3], Y. H. HUANG[3], Q. Q. LIANG[3], Y. F. XIE[3], Y. Y. CHEN[1,4]

[1]Chongqing Hospital of Traditional Chinese Medicine, Chongqing, China
[2]Shenzhen Hospital of Integrated Traditional Chinese and Western Medicine, Shenzhen, China
[3]Chongqing University of Posts and Telecommunications, Chongqing, China
[4]Bao'an Auchentic Traditional Chinese Medicine Therapy Hospital, Shenzhen, China

Yong Jiang and Hongzhuan Chen contributed equally to this work

Corresponding Author
Yuying Chen, MD; e-mail: eagle109@126.com

ABSTRACT – *Objective:* *Anthriscus sylvestris* (AS), a traditional medicinal herb, has emerged as a potential anti-cancer functional food. This study aimed to explore its anti-tumor mechanisms, focusing on colon cancer, using network pharmacology and experimental validation.

Materials and Methods: Active components of *Anthriscus sylvestris* were screened *via* the TCMSP database (OB ≥30%). Network pharmacology identified 91 shared targets between *Anthriscus sylvestris* and anti-tumor activity. Protein-protein interaction (PPI) networks, GO/KEGG analyses, and molecular docking were performed. *In vitro* experiments assessed the effects of *Anthriscus sylvestris* petroleum ether extract on STAT3 activity in HT29 colon cancer cells.

Results: Three key active components (dihydroanhydropodorhizol, dimethylmatairesinol, and (+)-hinokinin) were identified. Molecular docking revealed strong binding affinities (e.g., −7.84 kcal/mol for (+)-hinokinin-ESR1). KEGG enrichment highlighted pathways like FoxO and STAT3 signaling. In HT29 cells, AS extract concentration- and time-dependently suppressed STAT3/p-STAT3 protein expression (e.g., 80 μg/ml reduced STAT3 to 21.37% of control) and inhibited STAT3 DNA-binding activity (80 μg/ml: 21.37% inhibition).

Conclusions: *Anthriscus sylvestris* exerts anti-colon cancer effects by targeting STAT3 signaling, supported by network pharmacology and experimental validation. Its petroleum ether extract demonstrates significant therapeutic potential, providing a scientific foundation for developing AS-based anti-cancer foods or drugs.

KEYWORDS: *Anthriscus sylvestris*, Petroleum ether extract of *Anthriscus sylvestris*, Colon cancer, Anti-tumor activity, Network pharmacology.

INTRODUCTION

Anthriscus sylvestris (AS)[1] is a biennial or perennial herb belonging to the genus Anthriscus within the family Umbelliferae. It is traditionally recognized for its medicinal properties, including the enhancement of middle vital energy, lung tonification, asthma relief, blood stasis elimination, and blood regeneration. This

herb is predominantly used in treating conditions such as bruises, blood stasis, swelling, pain, spontaneous sweating, lung deficiency-induced coughing, spleen deficiency-induced abdominal distension, limb weakness, frequent urination in the elderly, edema, and menstrual irregularities in women. It is widely utilized as a tonic in folk medicine. Research on AS began in the 1970s and 1980s, with numerous scholars investigating its chemical composition. In recent years, research has increasingly focused on its pharmacological effects, particularly its anti-tumor activity. Tu Xianqin et al employed the MTT (Thiazolyl Blue Tetrazolium Bromide) colorimetric assay to demonstrate that various extracts of AS (including petroleum ether, chloroform, ethyl acetate, and nbutanol extracts) inhibited the proliferation of lung cancer cells A549 and H460. Similarly, Ma Xianghua found that the petroleum ether and ethyl acetate extracts of AS inhibited the proliferation of hepatocellular carcinoma cells HEPG2 and osteosarcoma cells MG-63. Lei Boting isolated and purified nine compounds from the petroleum ether extract of AS and screened them for their activity against colon cancer cells HT29 and SW620. The results indicated that lignans and phenylpropanoids in AS are among the main active constituents against colon cancer.

Colorectal cancer, often referred to as colon cancer or bowel cancer, is a malignant tumor of the gastrointestinal tract characterized by high morbidity and mortality rates[2]. Although current treatments are effective, they are frequently associated with severe adverse effects, drug resistance, and the risk of recurrence and metastasis, which can exacerbate patient suffering and diminish quality of life.

Traditional Chinese Medicine (TCM) serves as a significant adjuvant in tumor therapy, improving treatment efficacy, reducing drug resistance, and prolonging survival time. Persistent inflammatory responses play a crucial role in tumor development, and TCM's anti-inflammatory properties are vital in this context. However, the precise mechanisms underlying the anti-tumor activity of AS remain unclear.

In this study, we employed network pharmacology to analyze the active components of E. ginseng's anti-tumor activity, predict the core targets and pathways of these components, and preliminarily verify these targets through molecular docking. Given the significance of the JAK/STAT pathway in cancer development[3], this study aims to further validate E. ginseng's anti-cancer effects by examining its impact on STAT3 in colon cancer HT29 cells.

MATERIALS AND METHODS

Databases and software

TCMSP (https://old.tcmsp-e.com/tcmsp.php),
OMIM (https://www.omim.org), https://pubmed.ncbi.nlm.nih.gov/?term=OMIM
GeneCard (https://www.genecards.org/),
RCSB PDB (https://www.rcsb.org)
MetaScape (https://metascape.org/gp/index.html/main/step1),
STRING (https://cn.string-db.org/):
Software: Cytoscape 3.7.2, AutoDockTools 1.5.7, R 4.3.2, PyMOL 2.1.1.[4]

The selected databases and tools were employed to systematically explore the pharmacological mechanisms of traditional Chinese medicine compounds. TCMSP[5] provided a comprehensive repository for compound screening and target prediction, while OMIM[6] and GeneCard[7] collectively validated disease-associated genes and therapeutic targets. High-resolution protein structures from RCSB PDB[8] enabled molecular docking analysis using AutoDockTools and PyMOL for 3D interaction visualization. MetaScape and STRING facilitated functional enrichment and protein-protein interaction network construction, which were integrated and visualized *via* Cytoscape to map compound-target-pathway relationships. Statistical analyses, including GO and KEGG pathway enrichment, were performed using R 4.3.2 for robust data interpretation. This multi-platform approach synergistically supported network pharmacology and structure-based drug discovery, ensuring rigorous target identification, mechanistic validation, and systems-level analysis of bioactive components.

Screening of the main components of AS

The active ingredients of AS were obtained from the Traditional Chinese Medicine Systematic Pharmacology Database and Analysis Platform (TCMSP). Oral bioavailability (OB) refers to the rate and extent of drug absorption in the human body. The active ingredients of AS were selected based on an OB threshold of >30%[9]. The SmileName of the main component was input into SWISS Target Prediction, resulting in the identification of targets for AS.

Screening of tumor-related targets

The Swiss Target Prediction tool was employed to identify potential protein targets for small molecules. A comprehensive search and screening were then performed in the OMIM and GeneCards databases using "anti-tumor activity" as the keyword. The resulting targets were compiled, and duplicate entries were subsequently eliminated.

Construction of target Protein-Protein Interaction (PPI) Network

Venny 2.1 was utilized to map the intersection of the two sets of targets to understand the interactions between AS-related targets and tumor-related targets. The resulting intersection targets were uploaded to the STRING (Search Tool for the Retrieval of Interaction Genes) database[10], with Homo sapiens selected to obtain the protein interaction relationship. The file was downloaded in TSV format.

Subsequently, this file was imported into Cytoscape[11] 3.7.2 to construct a PPI network diagram. The CytoNCA plug-in in Cytoscape 3.7.2 was employed for further analysis of the topology of the PPI network and to filter out core targets within the PPI network diagram.

Functional analysis of GO and KEGG pathway

Bioinformatic enrichment analyses of the targets were conducted using the Metascape[12] platform, incorporating both Gene Ontology (GO) and Kyoto Encyclopedia of Genes and Genomes (KEGG) enrichment analyses. The GO analysis encompassed three domains: Biological Process (BP), Molecular Function (MF), and Cellular Component (CC). The results from the GO and KEGG analyses were prioritized based on *p*-values, with a significance threshold set at 0.01. The top 20 most relevant results that met these criteria were selected for further consideration.

Construction of a network diagram in AS

The network diagram depicting AS key active ingredients, anti-tumor activity targets, and signaling pathways was primarily created using Cytoscape 3.7.2. In this diagram, "node" represented AS components, or AS and anti-tumor targets, while "edge" denoted the relationship between the two nodes. The overall network diagram was analyzed using the Network Analyzer tool in Cytoscape, utilizing parameters such as Degree, Degree Centrality (DC), Betweenness Centrality (BC), and Closeness Centrality (CC). It can be used to analyze the relationship between key active components of AS and tumor targets.

Molecular docking simulation

The constructed AS key active ingredient-obesity disease target-signaling pathway network diagram was used to screen the active ingredients according to their numerical rankings. The targets with the top five-degree values were then screened in the PPI network diagram. The molecular structures of the active ingredients and key targets were obtained from the TCMSP and RCSB PDB databases. Following pre-processing of the ligand receptor by Autodock, molecular docking was initiated. The result with the lowest energy was taken for visual analysis and mapping of the binding sites by PyMOL. The results of the docking binding energies of the main active ingredients and core targets of AS were summarized and plotted as heat maps using the R programming language.

Study on the effect of AS on STAT3 in human colon cancer HT29 cells

BCA protein quantification

According to the number of standards and samples, the BCA reagent and Cu reagent were mixed in a ratio of 50:1 and stirred well to prepare the BCA working solution, which could be stabilized at room temperature for 24 hours. Take 10 µL of BSA standard, add PBS, and dilute to 100 µL to obtain the final concentration of 0.5 mg/mL standard. The standard was sequentially added to the protein standard wells of a 96-well plate by adding 0, 2, 4, 6, 8, 12, 16, and 20 µL, followed by adjusting the total volume to 20 µL using PBS. Appropriately diluted samples were added to the sample wells of the 96-well plate,

and 20 μL of samples were added to each well. Subsequently, 200 μL of BCA working solution was added to each well, followed by incubation at 37°C for 15-30 min. The A562nm value was detected using an enzyme marker, and then the protein concentration was calculated from the standard curve.

Western blot analysis

The BCA protein concentration kit was used to determine the protein concentration of the samples to obtain the sample volume, and after determining the sample volume, the samples were denatured in boiling water. Next, the gel-making step was carried out, and the sample, sample buffer, and internal control were added in order. Electrophoretic separation was then carried out. Subsequently, the PVDF membrane was activated with methanol, and a constant flow of membrane was carried out from the positive pole to the negative pole according to the order of membrane transfer. The transfected PVDF membrane was placed in a sealing solution at room temperature for 1 hour, after which the sealing solution was removed, diluted primary antibody was added, and the membrane was incubated at 4°C overnight. The diluted primary antibody solution was recovered and washed 3 times with TBST, followed by the addition of diluted secondary antibody solution and incubation at 37°C for 2 hours. Wash 3 times with TBST on a shaker at room temperature. The color development solution prepared under light-avoidance conditions was uniformly added to the PVDF membrane, which needed to be cleaned and placed on a plastic wrap, and after the appearance of the bands, the liquid on the membrane was removed, and the exposure was carried out in a dark room using a chemiluminescence gel imager, and the relative expression of the target protein was obtained by calculating the target protein integral optical density value/ internal control integral optical density value.

Electrophoretic mobility shift assay

Prepare the probe (STAT3: 5'-GATCCTTCTGGGAATTCCTAGATC-3'; Santa Cruz Biotechnology, Dallas, TX, USA). Labeling was performed using pierce's 3' end labeling kit (Pierce, Rockford, IL, USA), following the instructions. EMSA gel was configured, and DNA and protein were added to the spotting control in different combinations, plus a binding buffer. Next, electrophoresis was performed, and after electrophoresis, the film was removed and placed on a nylon membrane with a layer of moist blotting paper on the top and bottom, and then placed on a semi-dry setting of 100 V, 380 mA on a membrane transfer device for 1 hour. It was then fixed for 1 hour using a UV Crosslinker. The film is then washed using appropriate reagents, and the washed film is placed in an exposure cassette in a dark room, covered with X-ray film, and the exposure time is adjusted according to the temperature, frequently for 1 minute at room temperature. The film was then removed, developed, washed and fixed to obtain experimental results.

Statistical analysis

Pictures were drawn using GraphPad Prism 4.0. Comparisons of means between multiple groups were statistically analyzed using one-way analysis of variance (ANOVA); comparisons between the different groups and the control group were made using the Dunnett test. For comparison of the means of the two groups of data, the statistical analysis was performed using the paired *t*-test, $p < 0.05$ was statistically significant.

RESULTS

Screening of AS active ingredients and their targets

The active components of AS were obtained from the TCMSP database. By setting the condition OB≥30%, three effective active components were identified: Dihydroanhydropodorhizol, Dimethylmatairesinol, and (+)-hinokinin. By employing the SwissTargetPrediction database and setting the conditional probability to a value greater than 0, a total of 158 potential targets were identified.

Collection of action targets related to Anti-tumor activity and construction of a Venn diagram

A search of the OMIM database and GeneCards database for anti-tumor activity targets using the keyword 'Anti-tumor activity' yielded a total of 3049 targets related to anti-tumor activity. A further analysis was conducted using the Venny 2.1 online analysis tool, which identified a total of 91 AS targets with an intersection with anti-tumor activity. These are the potential AS targets for anti-tumor activity (Figure 1).

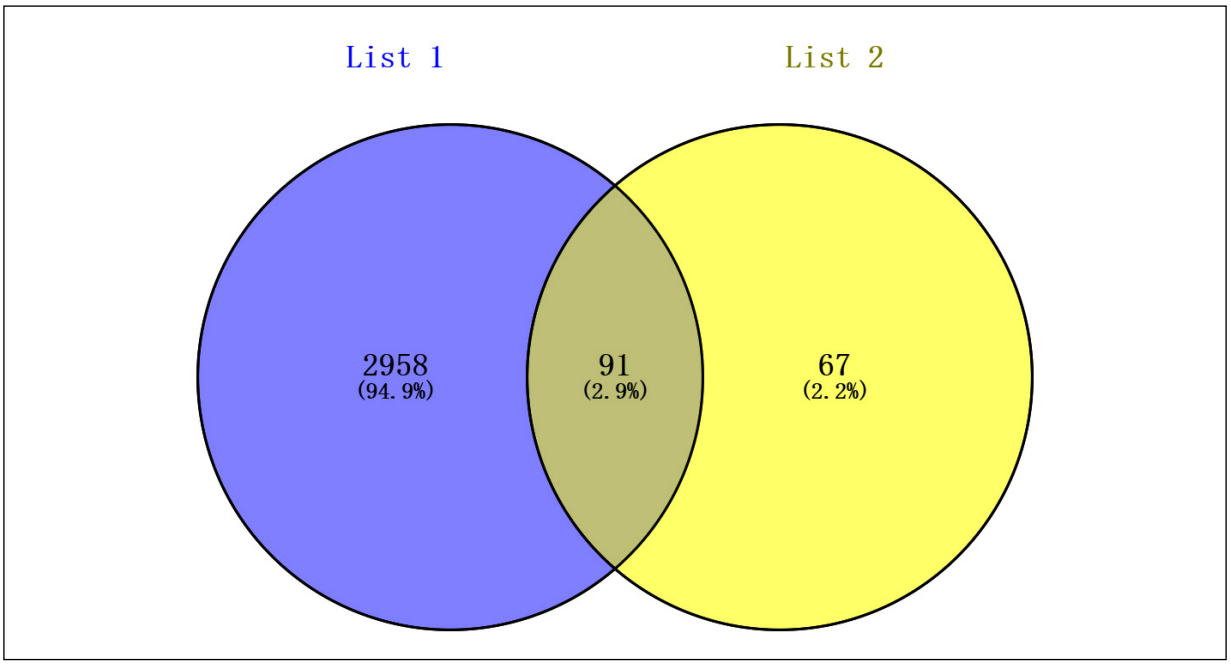

Figure 1. Intersection of anti-tumor targets (list1) and AS effective targets (list2) Venn diagrams.

Construction of Protein-Protein Interaction (PPI) network and screening of key targets of AS with potential intersecting targets of Anti-tumor activity

The data obtained on the 91 intersecting targets was submitted to the STRING database and subjected to PPI network analysis with the aim of identifying targets at key position nodes among the intersecting targets. The analysis results were saved as a (.TSV) format file, which was subsequently imported into Cytoscape 3.7.2 for the reconstruction of the target protein-protein interaction (PPI) network (Figure 2). The lines in the figure represent protein interactions. The triangles represent the drug AS, the squares represent the active substances of AS, and the circles represent the targets.

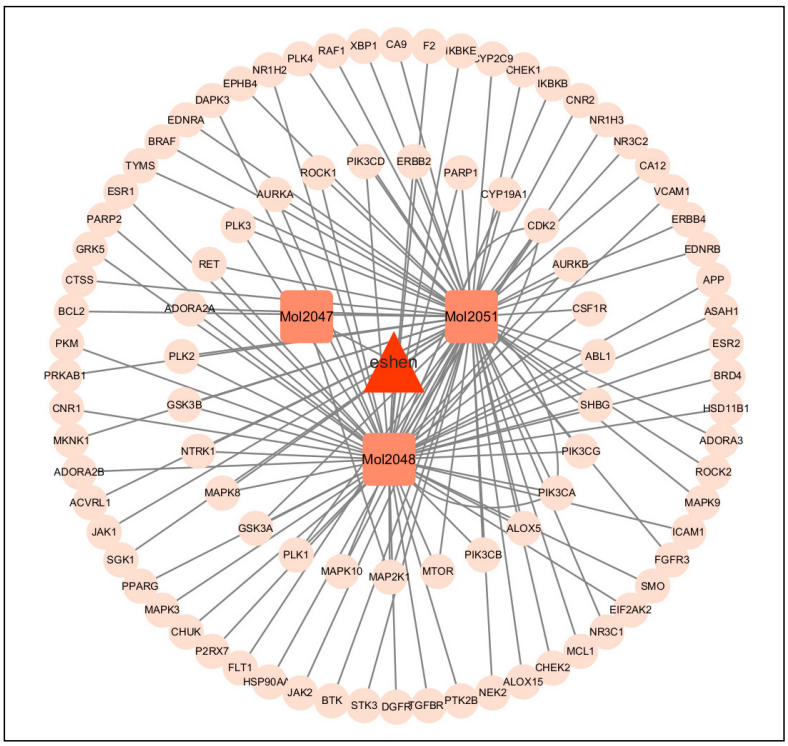

Figure 2. The target protein-protein interaction (PPI) network.

The diagram reveals that most targets for the key active ingredients of AS in anti-tumor activity have multiple network interactions. This indicates a diversity and complexity in the anti-tumor pathways of AS key active ingredients, as well as inter-pathway correlations. Key targets were identified by selecting those with degree, betweenness, and closeness values exceeding the average.

GO function and KEGG pathway enrichment analysis

GO pathway enrichment analysis

The Metascape platform was employed to identify intersecting targets with a *p*-value of less than 0.01. These targets were then analyzed by Gene Ontology (GO) for biological process (BP), molecular function (MF), and cellular component (CC). The resulting entries for BP were 1291, for CC items 80, and for MF 68. This yielded a total of 1439 enriched entries. The entries with the top ten logP values were displayed separately (Figure 3).

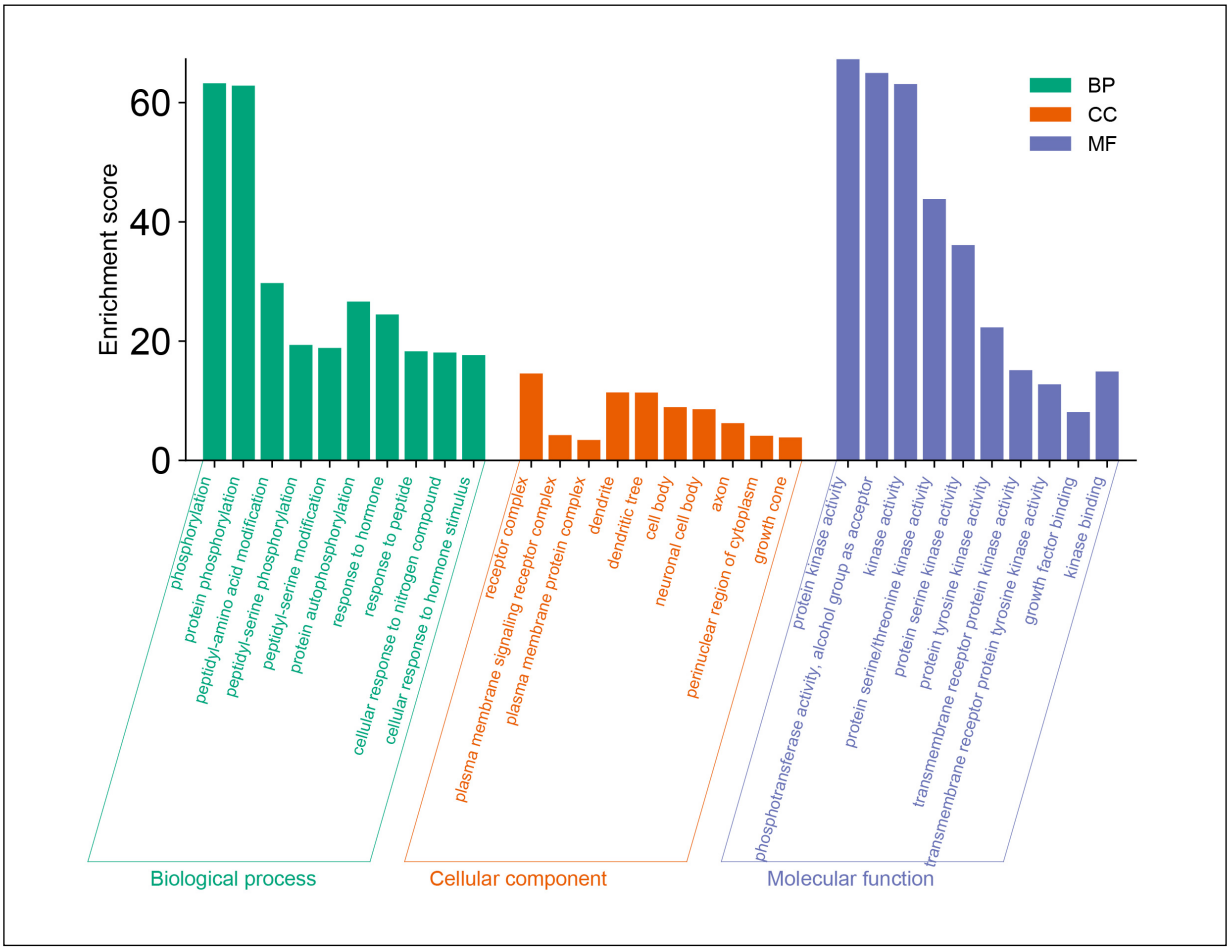

Figure 3. The top ten entries with logP values enriched by the GO channel.

The results of the BP analysis indicated that the principal biological processes associated with anti-tumor activity at the relevant targets are phosphorylation, protein autophosphorylation, response to hormones, positive regulation of the MAPK cascade, cellular activation, glandular development, positive regulation of programmed cell death, positive regulation of cell migration, positive regulation of cellular component biogenesis, and regulation of systemic processes.

The results of the CC experiments demonstrated that the principal cellular components of the relevant targets associated with anti-tumor activity were receptor complexes, dendrites, phosphatidylinositol 3-kinase complexes, class IA, transferring phosphorus-containing groups of the transferase complex,

centrosomes, membrane rafts, presynapses, nuclear membranes, Schaeffer's lateral branch-CA1 synapses, cytoplasmic side of plasma membranes, and so forth.

The results of the MF analysis indicate that the relevant targets possess molecular functions such as protein kinase activity, protein tyrosine kinase activity, kinase binding, protein serine/threonine/tyrosine kinase activity, nuclear receptor activity, 1-phosphatidylinositol-4-phosphate 3-kinase activity, non-transmembrane protein tyrosine kinase activity, IkappaB kinase activity, and protein homodimerization activity.

KEGG pathway enrichment analysis

The Metascape platform was employed to identify intersecting targets with a *p*-value of more than 0.01. These targets were subjected to KEGG analysis, resulting in the identification of 161 signal transduction pathways. The pathways with the top 10 logP values, from smallest to largest logP values, were presented in the form of bubble diagrams (Figure 4).

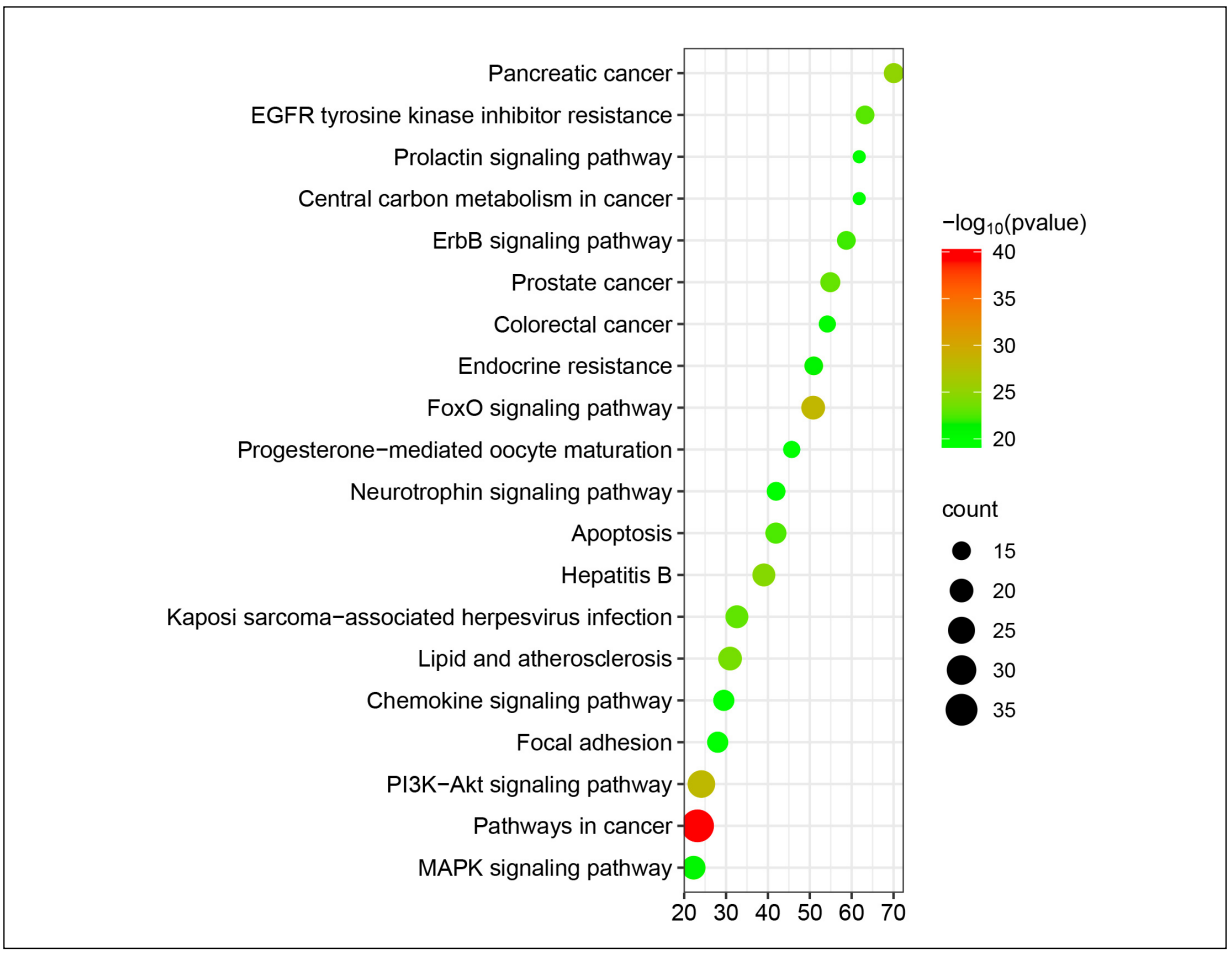

Figure 4. KEGG pathway enrichment bubble map.

The horizontal coordinate represents the degree of enrichment, with a larger value indicating a more significant pathway. The vertical coordinate represents the name of the function or pathway, with the size of the point reflecting the number of genes. A larger point indicates a greater number of genes, and the color reflects the size of the p-value. A redder color indicates a smaller *p*-value, which indicates high statistical significance. The above figure depicts the action-related targets, which are primarily associated with FoxO, Th17 cell differentiation, calcium signaling, NF-kappa B, hedgehog signaling, and other signaling pathways.

Construction of a network diagram of key active components, targets of Anti-tumor activity, and signaling pathways in AS

To further investigate the interactions among active components, targets, and signaling pathways in the mechanism of AS anti-tumor activity, a network diagram of key active components, anti-tumor activity targets, and signaling pathways of AS was constructed using Cytoscape 3.7.2 software (e.g., Figure 5).

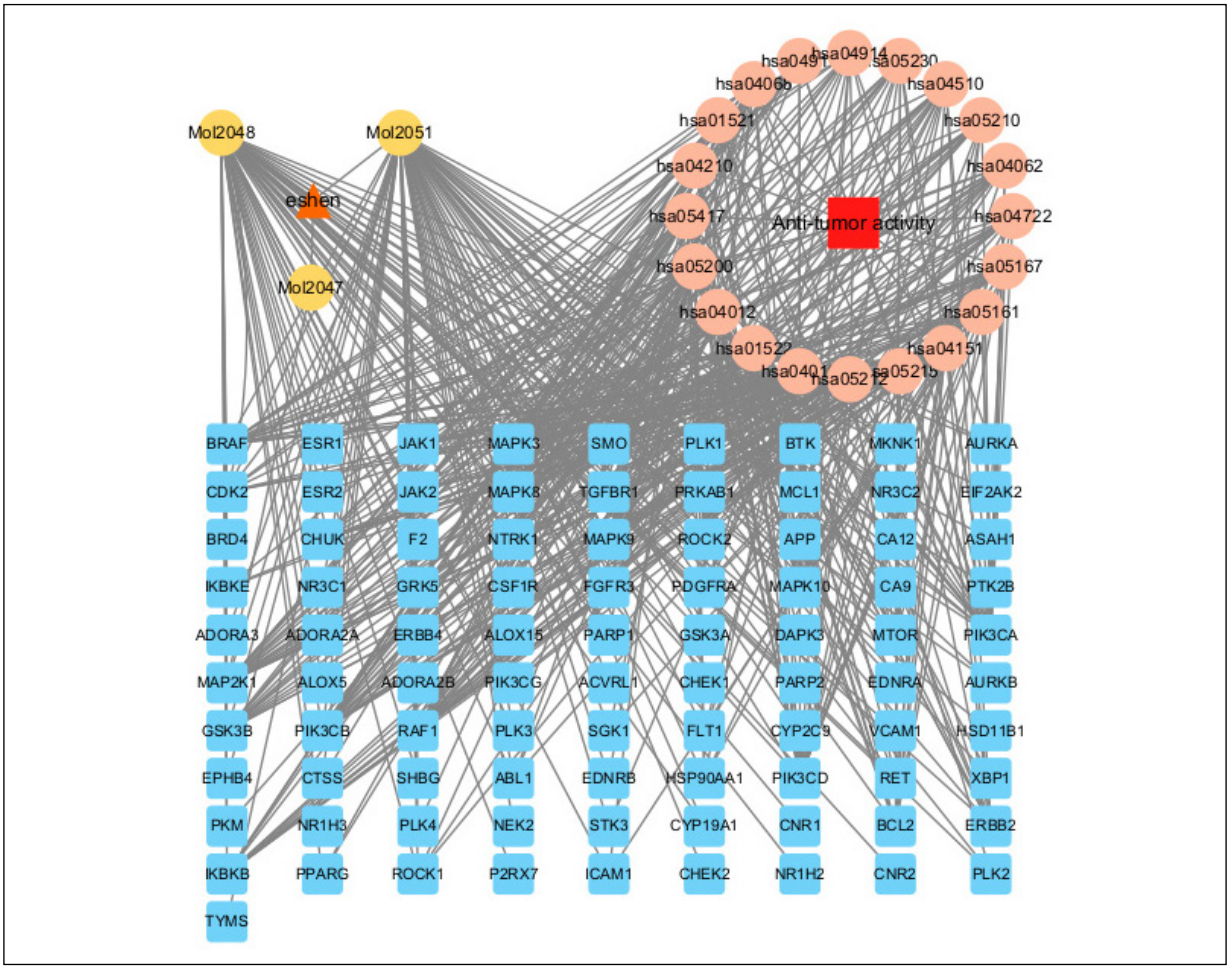

Figure 5. Network diagram of key active ingredients of AS - targets of Anti-tumor activity – signaling pathways.

The Metascape platform was employed to set a screening condition of $p < 0.01$, resulting in the identification of 161 signaling pathways derived from the BP, MF, and CC analyses of GO and KEGG analyses of the intersecting targets. The top 20 entries were then screened according to the LogP value. The target data for AS and the protein interactions of AS were imported into the Cytoscape Version 3.7.2 software, resulting in the construction of 116 nodes. Two software programs were employed to construct a diagram representing the relationships between drugs, components, diseases, targets, and pathways. The graph comprises 116 nodes, among which the triangular node represents the drug AS, three yellow circular nodes correspond to the active ingredients related to AS, the red square nodes relate to the diseases associated with anti-tumor activity, 91 blue square nodes represent the targets related to the anti-tumor activity of AS, and 20 pink circular nodes correspond to the enriched pathways. The 504 edges represent the action relationships among the nodes. A topological analysis of the network was conducted using the built-in CytoNCA plug-in, resulting in the following findings: The Degree value of (+)-Hinokinin was 65, its Betweenness Centrality was 5249.975, and its Closeness Centrality was 0.5837563. The Degree value of Dihydroanhydropodorhizol was 2, its Betweenness Centrality was 2.0482094, and its Closeness Centrality was 0. The Degree value of 35825545 and the Closeness Centrality of 59 for Di-

methylmatairesinol indicate that the active ingredients (+)-hinokinin and Dimethylmatairesinol played an important role in the anti-tumor activity. The Degree value was 4451.399, with a Closeness Centrality of 0.5502392. This suggests that the active component, (+)-Hinokinin, Dimethylmatairesinol, plays an important role in the process of anti-tumor activity (Figure 6).

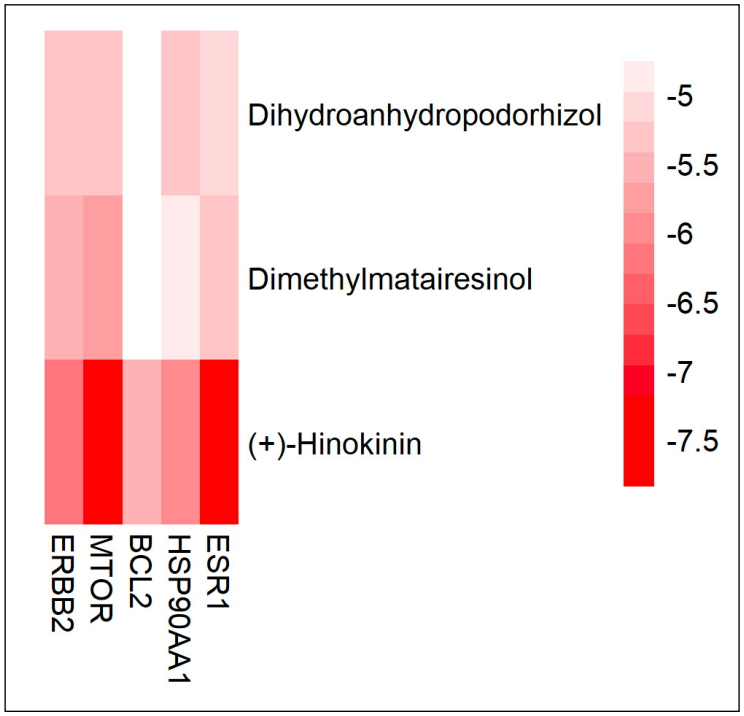

Figure 6. Thermogram of molecular docking binding energy (kcal/mol) of AS active ingredients with corresponding core targets.

Molecular docking analysis

The key active components of AS – anti-tumor activity targets – signaling pathways were constructed in 2.5 and sorted according to degree value. The top three components were then screened out, namely Dihydroanhydropropodorhizol, Dimethylmatairesinol, and (+)-Hinokinin, which were identified as three active components. The sdf files were downloaded from the PubChem database (https://pubchem.ncbi.nlm.nih.gov/) and their structures were optimized by Open Babel 3.1.1. The targets subjected to screening were BCL2, HSP90AA1, ESR1, ERBB2, and MTOR. The molecular structures of the key targets were then obtained from the RCSB PDB database[8] (https://www.rcsb.org/), and the target protein receptors were subjected to water molecule removal and ligand removal operations by PyMol 2.5.0. Molecular docking was performed with AutoDockTools 1.5.7[13], taking the result with the largest absolute value of the binding energy, which is usually considered to be good if the binding energy is less than -5.0 kJ/mol, and less than 0 kJ/mol is considered to be docked in the natural state. The binding sites were analyzed and mapped visually using PyMOL. The results of 15 molecular docking experiments of the key active components of AS with the key targets are presented in Table 1.

Table 1. Molecular docking binding energies of key active components of AS with corresponding core targets (kcal/mol).

Active Ingredients	ERBB2 (3P0Y)	MTOR (4O25)	HSP90AA1 (ST10)	BCL2 (8G3S)	ESR1 (6PSJ)
Dihydroanhydropodorhizol	-5.21	-5.41	-4.72	-5.25	-5.11
Dimethylmatairesinol	-5.43	-5.82	-4.54	-4.77	-5.38
(+)-Hinokinin	-6.1	-7.58	-5.5	-5.97	-7.84

The results demonstrated that the three active ingredients exhibited binding energies of less than -5.0 kJ/mol with each target, indicating that the key active ingredients in AS exhibited superior binding abilities and binding affinities with each key target. The docking binding energies of (+)-Hinokinin with MTOR and (+)-Hinokinin1 with ESR1 were -7.58 kcal/mol and -7.84 kcal/mol, respectively, indicating that the components exhibited a high binding ability to the targets. The molecular docking diagram is presented in Figure 6. The aforementioned molecular docking experimental results validated the accuracy of the network pharmacological screening (Figure 7).

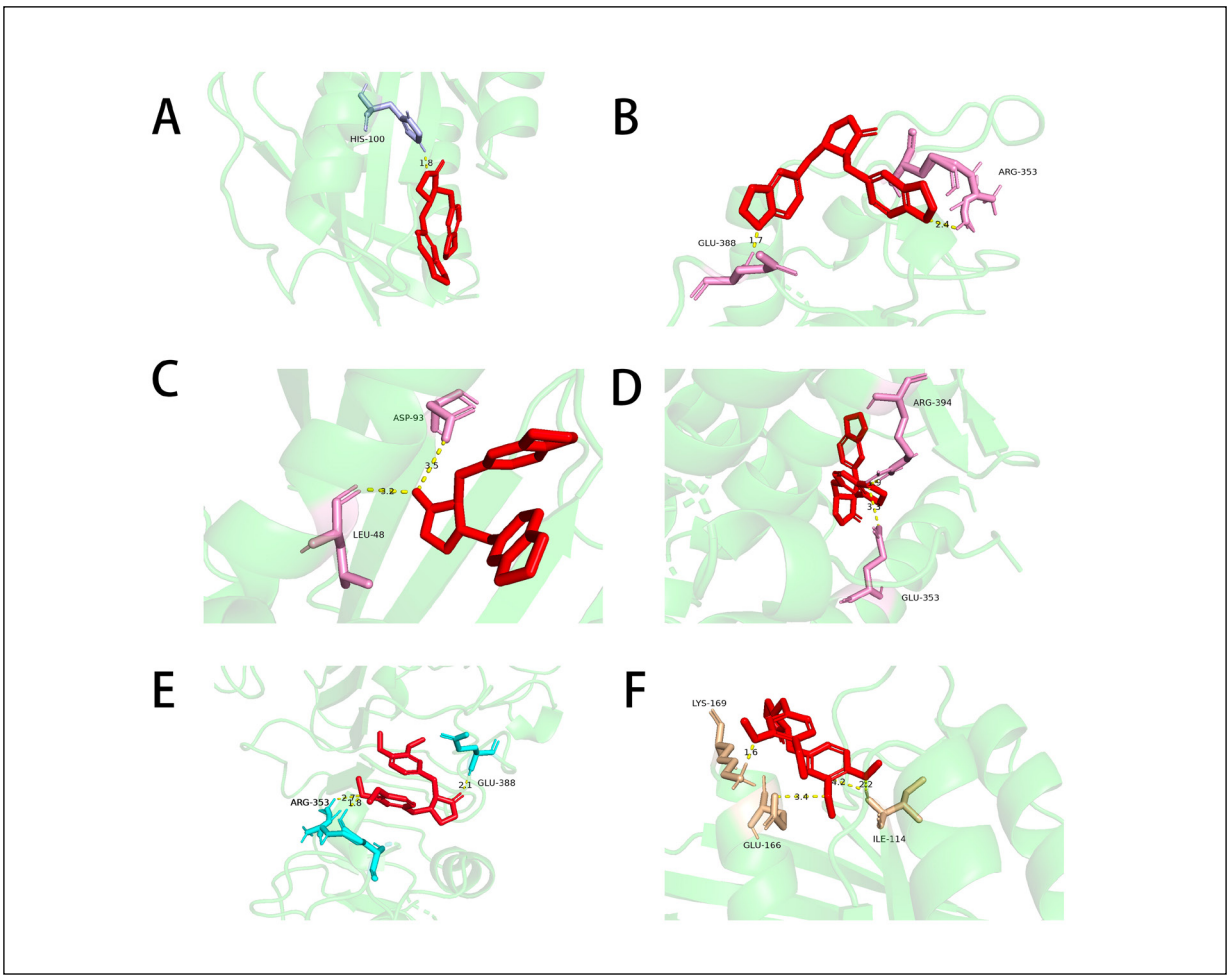

Figure 7. Molecular docking diagram of key active components of AS and core targets. *A*, MTOR(4O25) with (+)-Hinokinin. *B*, ERBB2(3P0Y) with (+)-Hinokinin. *C*, HSP90AA1(3T10) with (+)-Hinokinin. *D*, ESR1(6PSJ) with (+)-Hinokinin. *E*, ERBB2(3P0Y) with Dimethylmatairesinol. *F*, MTOR(4O25) with Dimethylmatairesinol.

THE EFFECT OF THE EXTRACT OF AS ON STAT3 IN COLON CANCER HT29 CELLS

Effect of AS extracts on STAT3 activity in HT-29 human colon cancer cells and quantitative-effect relationship

After HT-29 human colon cancer cells were first cultured at a density of 1×10^5 per well, HT-29 human colon cancer cells were first used to investigate the effects of different concentrations of petroleum ether extracts of eglantine, and it was found that different concentrations of AS petroleum ether extract had different effects on the protein expression of STAT3 and p-STAT3, which showed a trend that the higher the concentration, the more the protein expression was inhibited. Table 2 shows the raw data of STAT3 and p-STAT3 protein expression from the total protein concentration of the extracted cells, and the related bands are shown in Figure 8.

Table 2. Expression of STAT3 and p-STAT3 proteins in HT-29 human colon cancer cells at different concentrations of AS petroleum ether extract group.

Groups	STAT3	*p*-STAT3
Concentration of petroleum ether in AS 0μg/ml (5)	3.0321	3.1258
Concentration of petroleum ether in AS 10μg/ml (4)	2.6539	2.7949
Concentration of petroleum ether in AS 20μg/ml (3)	1.8100	2.2930
Concentration of petroleum ether in AS 40μg/ml (2)	1.4247	1.5126
Concentration of petroleum ether in AS 80μg/ml (1)	1.0000	1.0000

Figure 8. Expression of STAT3 and pSTAT3 proteins in HT-29 human colon cancer cells at different concentrations of AS petroleum ether extract.

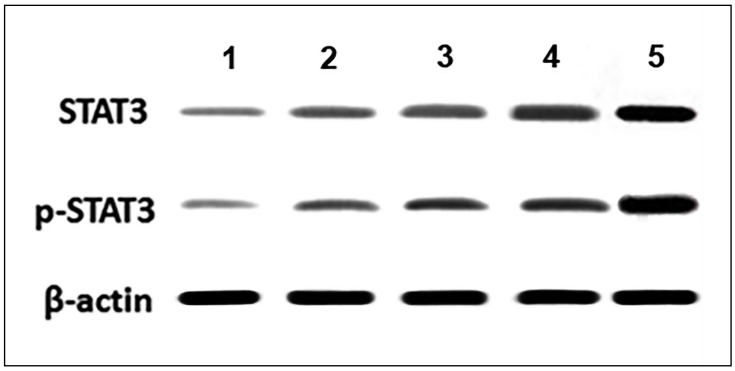

Effect of AS extract on STAT3 binding activity in human colon cancer HT29 cells

HT29 cells were inoculated in sterile 6-well plates at a density of 1×10^5 cells/well and placed in an incubator at constant temperature for 48 h. After removing the cells, the nuclear proteins of the cells were extracted by adding a culture medium containing petroleum ether extracts of AS at different concentrations for 24 h. The cells were then incubated for 24 h in a culture medium containing petroleum ether extracts of Epsom ginseng at different concentrations. The electrophoretic mobility shift assay showed that the DNA binding activity of STAT3 within the nuclear protein of human colorectal cancer HT29 cell source was strongly positive. The treatment of AS extract significantly inhibited the DNA-binding activity of STAT3, and the DNA-binding activity of STAT3 within the nuclear proteins of HT29 cell source was significantly reduced with increasing concentrations of AS extract in a concentration-dependent manner (Table 3, Figures 9 and 10).

Table 3. Inhibitory effect of AS extract on STAT3 binding activity in HT29 cells.

AS extract concentration	0μg/ml	10μg/ml	20μg/ml	40μg/ml	80μg/ml
	100±1.03	83.23±3.82	70.49±2.24	42.38±4.97	21.37±4.57

Chronotropic modulation of STAT3 activity in human colon cancer HT29 cells by AS extracts

HT29 cells were inoculated in sterile 6-well plates at a density of 1×105 cells/well, placed in the incubator for 48h at a constant temperature, and total cell protein extraction was carried out after removing the cells and adding 40μg/ml AS petroleum ether extract to the incubation solution for 0h, 6h, 12h, 24h, and 36h. The results after Western blot analysis showed that 40μg/ml AS petroleum ether extract significantly inhibited the expression of STAT3 and p-STAT3 in HT29 cells, and this inhibitory effect was gradually increased with the time of incubation in a time-dependent manner (Figures 11, 12, and Table 4).

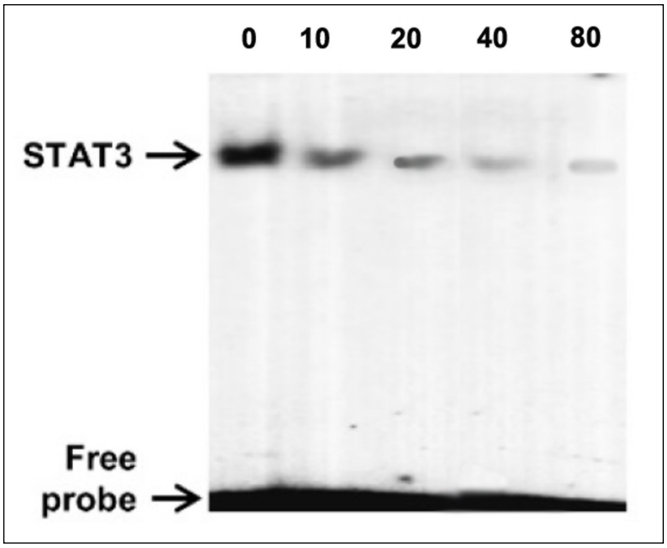

Figure 9. Analysis of DNA-binding activity of STAT3 within HT29 cytosolic proteins.

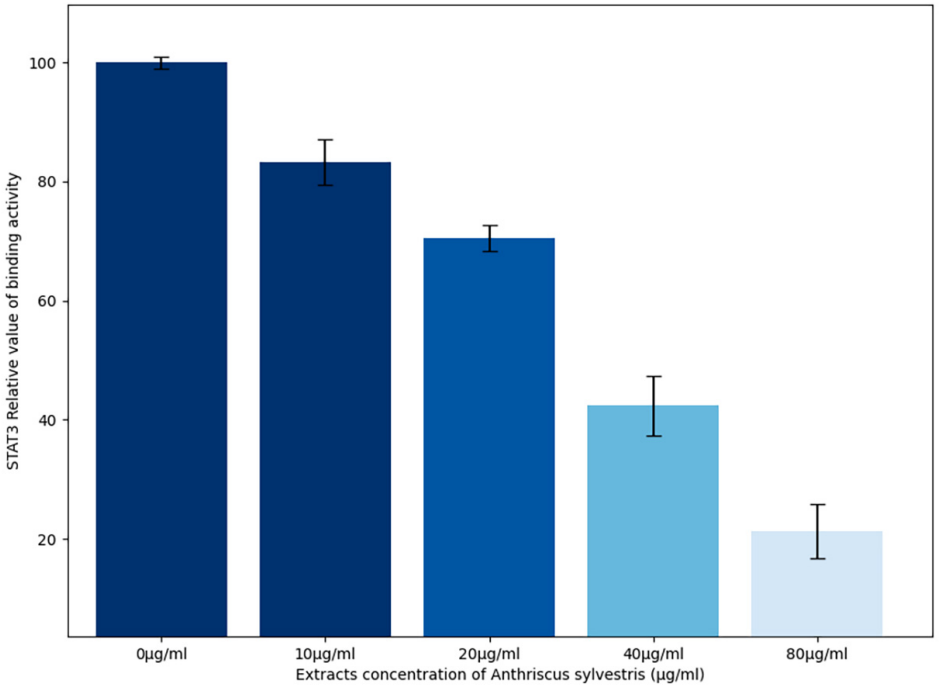

Figure 10. Effect of AS extract on STAT3 binding activity in HT29 cells.

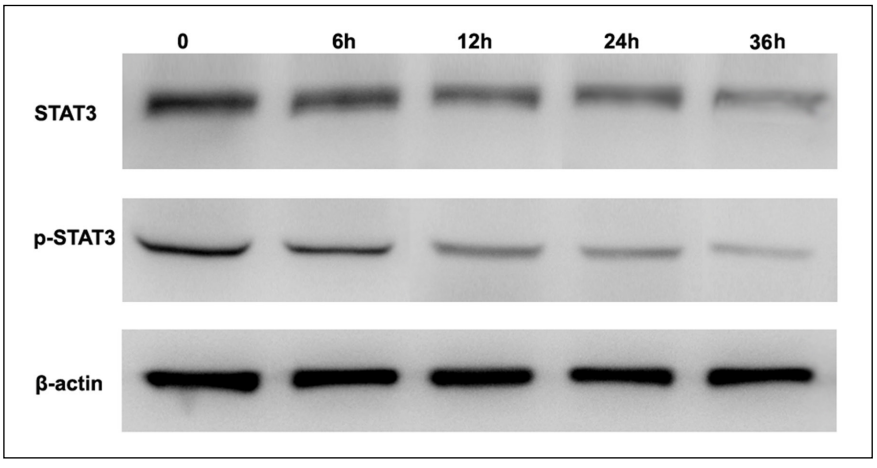

Figure 11. 40μg/ml AS petroleum ether extract significantly inhibited STAT3 activity in HT29 cells.

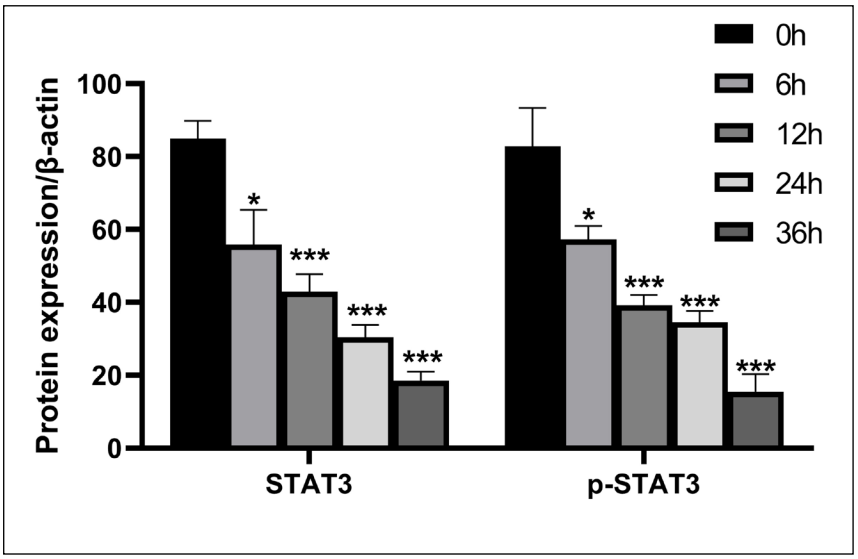

Figure 12. 40μg/ml AS petroleum ether extract significantly inhibited STAT3 activity in HT29 cells.

Table 4. 40μg/ml AS petroleum ether extract significantly inhibits STAT3 activity in HT29 cells Data Records.

Processing time	STAT3	p-STAT3
0h	84.99±4.79	82.83±10.552
6h	55.89±9.51	57.31±3.66
12h	42.99±4.76	39.24±2.82
24h	30.46±3.32	34.53±3.05
36h	18.569±2.42	15.50±4.79

DISCUSSION

In the present study, we employed network pharmacology to elucidate the potential molecular mechanisms underlying the anti-tumor effects of the primary active ingredients of AS. Three active compounds – dihydrodehydropyrazole, dimethylstrychnine ethanol, and (+)-hinokiin – were identified from the Traditional Chinese Medicine Systems Pharmacology Database and Analysis Platform (TCMSP). Their potential targets were predicted using the Swiss Target Prediction tool. These active compounds exhibited high oral bioavailability (OB >30%), indicating favorable in vivo absorption and potential therapeutic efficacy.

Anti-tumor-related targets were identified through the Online Mendelian Inheritance in Man (OMIM) and GeneCards databases, resulting in a total of 91 intersecting targets for the benzoin active ingredients. Protein-protein interaction (PPI) network analysis highlighted the intricate interactions among these targets, allowing for the identification of key central targets. Gene Ontology (GO) and Kyoto Encyclopedia of Genes and Genomes (KEGG) pathway enrichment analyses demonstrated that these targets are significantly involved in various biological processes, molecular functions, and cellular components. Notably, the identified targets are implicated in critical biological processes such as cell signaling, apoptosis, and cell cycle regulation, underscoring the complex interplay between the active ingredients of Astragalus and their respective targets.

In the network of signaling pathways associated with the anti-tumor activity of Asparagus ginseng's key active ingredients, the identified targets include BCL2, HSP90AA1, ESR1, ERBB2, and MTOR. Molecular docking simulations confirmed the binding affinity of the main active components of Asparagus ginseng to several anti-tumor targets. The analysis revealed that (+)-rhinoceratin exhibits a strong binding affinity to mTOR and ESR1, aligning with its potential anti-tumor effects[14]. These findings provide a

theoretical foundation for the potential use of Asparagus ginseng as an anti-cancer agent. Studies have indicated that Bcl2 expression can be regulated by the upstream transcription factor STAT3[15]. The STAT3 pathway is positively modulated by mTOR signaling, and Hsp90AA1 interacts with STAT3 and caveolin-1 in plasma membrane rafts to influence cell signaling[16]. EGFR, an upstream receptor of the STAT family, is a member of the ERBB family and plays a critical role in cell proliferation and tumor development[17].

Based on the primary target, we selected a transcription factor capable of interacting with multiple others for experimental validation. STAT3, a member of the Signal Transducer and Activator of Transcription (STAT) family, is a key signaling molecule involved in oncogenesis, immune regulation, and inflammatory responses. STAT3 activates the Janus Kinase/Signal Transducer and Activator of Transcription (JAK/STAT) signaling pathway[18]. It is classified as a proto-oncogene and is detectable in various malignancies. The STAT3-associated pathway is crucial in tumor-related inflammation, inducing the expression of several inflammation-related genes. Upon phosphorylation, STAT3 molecules dimerize, translocate to the nucleus, bind specific DNA sequences, and promote the transcription of genes related to proliferation and anti-apoptosis, including Bcl-2, Bcl-xl, IL-17, IL-23, MCL-1, and survivin. Additionally, activated STAT3 enhances tumor angiogenesis by regulating hypoxia-inducible factor-1 (HIF-1) and vascular endothelial growth factor (VEGF) expression. Consequently, STAT3 represents a potential therapeutic target for cancer. Research indicates that genetic interference with STAT3 expression induces tumor cell apoptosis. Substantial evidence supports that inhibiting STAT3 activation through inhibitors or gene knockout systems offers a promising therapeutic approach for cancer and other diseases. STAT3 inhibitors exert anti-tumor effects via two primary mechanisms: blocking the upstream pathway of STAT3 and directly targeting the STAT3 protein itself.

To investigate the role of Asparagus ginseng (AS) extract, we cultured colon cancer HT29 cells and examined the alterations in STAT3 and phosphorylated STAT3 (p-STAT3) protein expression induced by AS petroleum ether extract. In normal cells, transient activation of STAT3, typically through phosphorylation, relays cytokine and growth factor receptor signals from the plasma membrane to the nucleus. As a transcription factor, STAT3 regulates genes associated with cell survival, proliferation, angiogenesis, invasion, metastasis, drug resistance, and immune evasion. Overexpression of STAT3 has been documented in various patient-derived tumor tissues. Our study found that increasing concentrations of AS petroleum ether extract in cancer cells enhanced the inhibitory effect on STAT3 and p-STAT3 proteins. The DNA-binding activity of STAT3 was detected in nuclear proteins and was strongly positive. However, the DNA-binding activity of STAT3 in nuclear proteins extracted from HT29 cells significantly decreased in a concentration-dependent manner with increasing concentrations of the AS extract. Additionally, prolonged cell culture time resulted in a gradual decrease in STAT3 activity in HT29 cells, confirming the inhibitory effect of AS extract on STAT3. These findings suggest that AS extract can serve as a potential anti-cancer agent for the treatment of colon cancer.

In summary, this study screened potential active ingredients and targets through network pharmacology. The interaction and binding mode of the target were revealed through the PPI network and molecular docking simulation. Finally, this experiment confirmed that AS extract does have an inhibitory effect on STAT3 and can inhibit colon cancer tumor cells. However, further research on the mechanism of AS inhibiting intestinal cancer is needed.

CONCLUSIONS

In this study, we investigated the anti-tumor activity of AS and the impact of its petroleum ether extract on STAT3 in human colon cancer HT29 cells. The results indicated that the active components contained in AS can inhibit the growth of tumor cells through various mechanisms. Specifically, we identified 3 active ingredients, 91 targets, and 161 disease-related signal pathways. The enrichment analysis of the KEGG pathway revealed that Dihydroanhydropodorhizol, Dimethylmatairesinol, and (+)-hinokitiin are closely associated with anti-tumor activity. Molecular docking results demonstrated a high binding affinity of AS components to their targets. Furthermore, we observed that the expression of STAT3 and p-STAT3 proteins was progressively inhibited with increasing concentrations of AS petroleum ether extract. Electrophoretic mobility analysis showed that the AS extract significantly suppressed the DNA-binding activity of STAT3. Western blot analysis also revealed that 40 μg/ml of AS petroleum ether extract could significantly inhibit the expression of STAT3 and p-STAT3 in HT29 cells.

In conclusion, this study integrates network pharmacology and molecular docking to identify key anti-tumor components (e.g., (+)-hinokinin) and targets (e.g., STAT3) in AS, with experimental validation demonstrating dose- and time-dependent STAT3 suppression in colon cancer cells. While the interdis-

ciplinary approach combining bioinformatics, computational tools, and cellular assays provides novel insights into STAT3 pathway modulation and establishes a framework for herbal medicine research in oncology, limitations persist. Notably, network-predicted targets (e.g., BCL2, MTOR) and pathways (e.g., FoxO, NF-κB) lack experimental validation, and the absence of pharmacokinetic or toxicity assessments limits translational relevance. Despite these gaps, the work bridges traditional medicinal applications with modern molecular mechanisms, highlighting the plant's potential as an anti-cancer agent.

Ethics approval:

This study did not involve animal experimentation; thus, formal ethical approval was not required. All procedures strictly adhered to institutional and national guidelines for non-animal research.

Informed consent:

This study did not involve human participants, patient data, or clinical interventions; therefore, informed consent was not required. All research activities complied with institutional and national ethical guidelines for non-human studies.

Funding:

This work was co-supported by the National Natural Science Foundation of China (NSFC) (No. 81773954).

CRediT authorship contribution statement:

Jian-zhong Shu: Writing – Original Draft, Conceptualization, Methodology, Validation, Investigation, Resources, Visualization. Yong Jiang: Writing – Original Draft, Conceptualization, Methodology, Validation, Investigation, Resources, Visualization. Hong-zhuan Chen: Investigation, Resources, Writing – Original Draft, Visualization. Feng-ying Liu: Methodology, Formal analysis, Writing – Original Draft, Writing – Review & Editing, Visualization. Yu-han Huang: Methodology, Formal analysis, Writing – Original Draft, Writing – Review & Editing, Visualization. Qian-qian Liang: Methodology, Formal analysis, Writing – Original Draft, Writing – Review & Editing, Visualization. Yong-fang Xie: Conceptualization, Project administration, Funding acquisition. Yu-ying Chen: Conceptualization, Project administration, Funding acquisition.

ORCID:

Jian-zhong Shu: 0009-0000-8412-8834. Yong Jiang: 0000-0002-3609-2280. Hong-zhuan Chen: 0009-0005-5272-200X. Feng-ying Liu: 0009-0006-0788-8649. Yu-Han Huang: 0009-0000-2222-2796. Qian-qian Liang: 0009-0007-8118-1083. Yong-fang Xie: 0000-0002-8210-5732. Yu-ying Chen: 0009-0000-1849-3278

Conflict of interest:

The authors declare that they have no conflict of interest to disclose.

REFERENCES

1. Orčić D, Berežni S, Mimica-Dukić N. Quantitative HPLC-UV Study of Lignans in Anthriscus sylvestris. Molecules 2022; 27: 6072.
2. Zhang M, Ji X, Li Y, Chen X, Wu X, Tan R, Jiang H. Anthriscus sylvestris: An overview on Bioactive Compounds and Anticancer Mechanisms from a Traditional Medicinal Plant to Modern Investigation. Mini Rev Med Chem 2024; 24: 1162-1176.
3. Grivennikov S, Karin E, Terzic J, Mucida D, Yu GY, Vallabhapurapu S, Scheller J, Rose-John S, Cheroutre H, Eckmann L, Karin M. IL-6 and Stat3 are required for survival of intestinal epithelial cells and development of colitis-associated cancer. Cancer Cell 2009; 15: 103-113.
4. Shu J-Z, Li Y-H, Pu Y-Q, Liu Q-L, Zhang J, Gan Y-L, Xie Y-F. Study on hypoglycemic mechanism of Radix Puerariae based on network pharmacology. China Mod Med 2022; 29: 11-14.
5. Ru J, Li P, Wang J, Zhou W, Li B, Huang C, Li P, Guo Z, Tao W, Yang Y, Xu X, Li Y, Wang Y, Yang L. TCMSP: a database of systems pharmacology for drug discovery from herbal medicines. J Cheminform 2014; 6: 13.
6. Amberger JS, Hamosh A. Searching Online Mendelian Inheritance in Man (OMIM): A Knowledgebase of Human Genes and Genetic Phenotypes. Curr Protoc Bioinforma 2017; 58: 1.2.1-1.2.12.
7. Rappaport N, Fishilevich S, Nudel R, Twik M, Belinky F, Plaschkes I, Stein TI, Cohen D, Oz-Levi D, Safran M, Lancet D. Rational confederation of genes and diseases: NGS interpretation via GeneCards, MalaCards and VarElect. Biomed Eng Online 2017; 16(Suppl 1): 72.
8. Bittrich S, Bhikadiya C, Bi C, Chao H, Duarte JM, Dutta S, Fayazi M, Henry J, Khokhriakov I, Lowe R, Piehl DW, Segura J, Vallat B, Voigt M, Westbrook JD, Burley SK, Rose Y. RCSB Protein Data Bank: Efficient Searching and Simultaneous Access to One Million Computed Structure Models Alongside the PDB Structures Enabled by Architectural Advances. J Mol Biol 2023; 435: 167994.

9. Liu H, Wang J, Zhou W, Wang Y, Yang L. Systems approaches and polypharmacology for drug discovery from herbal medicines: an example using licorice. J Ethnopharmacol 2013; 146: 773-793.
10. Szklarczyk D, Kirsch R, Koutrouli M, Nastou K, Mehryary F, Hachilif R, Gable AL, Fang T, Doncheva NT, Pyysalo S, Bork P, Jensen LJ, von Mering C. The STRING database in 2023: protein-protein association networks and functional enrichment analyses for any sequenced genome of interest. Nucleic Acids Res 2023; 51(D1): D638-D646.
11. Shannon P, Markiel A, Ozier O, Baliga NS, Wang JT, Ramage D, Amin N, Schwikowski B, Ideker T. Cytoscape: a software environment for integrated models of biomolecular interaction networks. Genome Res 2003; 13: 2498-2504.
12. Zhou Y, Zhou B, Pache L, Chang M, Khodabakhshi AH, Tanaseichuk O, Benner C, Chanda SK. Metascape provides a biologist-oriented resource for the analysis of systems-level datasets. Nat Commun 2019; 10: 1523.
13. Zhang Y, Sanner MF. AutoDock CrankPep: combining folding and docking to predict protein-peptide complexes. Bioinformatics 2019; 35: 5121-5127.
14. Wu D, Wang Z. Gastric Cancer Cell-Derived Kynurenines Hyperactive Regulatory T Cells to Promote Chemoresistance via the IL-10/STAT3/BCL2 Signaling Pathway. DNA Cell Biol 2022; 41: 447-455.
15. Shen J, Zhang Y, Wu X. Rapamycin promotes hematoma resorption and enhances endothelial cell function by suppressing the mTOR/STAT3 signaling in chronic subdural hematoma. Exp Cell Res 2023; 433: 113829.
16. Shah M, Patel K, Fried VA, Sehgal PB. Interactions of STAT3 with caveolin-1 and heat shock protein 90 in plasma membrane raft and cytosolic complexes. Preservation of cytokine signaling during fever. J Biol Chem 2002; 277: 45662-45669.
17. Chen M, Obasanmi G, Armstrong D, Lavery NJ, Kissenpfennig A, Lois N, Xu H. STAT3 activation in circulating myeloid-derived cells contributes to retinal microvascular dysfunction in diabetes. J Neuroinflammation 2019; 16: 138.
18. Gharibi T, Babaloo Z, Hosseini A, Abdollahpour-Alitappeh M, Hashemi V, Marofi F, Nejati K, Baradaran B. Targeting STAT3 in cancer and autoimmune diseases. Eur J Pharmacol 2020; 878: 173107.